N79-30356

# ERRATA

NASA Technical Memorandum 79227

THE EROSION/CORROSION OF SMALL SUPERALLOY TURBINE ROTORS OPERATING IN THE EFFLUENT OF A PFB COAL COMBUSTOR

G. R. Zellars, S. M. Benford, A. P. Rowe, and C. E. Lowell

July 30, 1979

Page 2, paragraph 2, lines 1, 2, and 3:

The sentence beginning The NASA Lewis PFBC research program,

should be changed to read:

The NASA Lewis PFBC research program in the areas of coal combustion and turbine and materials technology was initiated in 1976 as part of NASA's Energy Technology Identification and Verification programs.

NASA Technical Memorandum 79227



# THE EROSION/CORROSION OF SMALL SUPERALLOY TURBINE ROTORS OPERATING IN THE EFFLUENT OF A PFB COAL COMBUSTOR

G. R. Zellars, S. M. Benford,
A. P. Rowe, and C. E. Lowell
Lewis Research Center
Cleveland, Ohio


Prepared for the
Advanced Materials for Alternate Fuel Capable
Directly Fired Heat Engines Conference
cosponsored by the United States Department of Energy
and the Electric Power Research Institute
Castine, Maine, July 30 - August 3, 1979

# THE EROSION/CORROSION OF SMALL SUPERALLOY TURBINE ROTORS OPERATING IN THE EFFLUENT OF A PFB COAL COMBUSTOR

G. R. Zellars, S. M. Benford, A. P. Rowe and C. E. Lowell
National Aeronautics and Space Administration

## ABSTRACT

Integrally cast Alloy 713LC and IN792 + Hf superalloy turbine rotors in a single stage turbine with 6% partial admittance have been operated in the effluent of a pressurized fluidized bed coal combustor for up to 164 hours. Total mass flow was 300 kg/hr and average particulate loadings ranged from 600 to 2800 ppm for several coal/sorbent combinations. A 5.5 atm turbine inlet gas pressure and inlet gas temperatures from 700 to 800C yielded absolute gas velocities at the stator exit of about 500 m/s. The angular rotation speed (40,000 RPM) of the 6 inch diameter rotors was equivalent to a tip speed of about 300 m/s, and average gas velocities relative to the rotating surface ranged from 260 to 330 m/s at mean radius.

The rotor erosion pattern reflects heavy particle separation with severe (5 to 500 cm/yr) erosion at the leading edge, pressure side center, and suction side trailing edge at the tip. The erosion distribution pattern provides a spectrum of erosion/oxidation/deposition as a function of blade position. This spectrum includes enhanced oxidation (10 to 100 x air), mixed oxides in exposed depletion zones, sulfur rich oxides in deposition zones, and rugged areas of erosive oxide removal. Although particle separation and erosive damage will be much less severe in large turbines operated at lower particulate levels, these data suggest that preferential degradation paths may exist even under the targeted lower loadings ($<$20 ppm) because of the diversity of potential erosion/corrosion interactions along erosion paths.

## INTRODUCTION

The operation of a turbine in the effluent of a pressurized fluidized bed coal combustor (PFBC) presents serious materials problems. Previous turbine tests in coal fired plants indicated that coal ash can be severely erosive (1,2). The presence of sulfur and alkali impurities in PFB emission gases, even after significant removal of $SO_x$ by $CaCO_3$ and MgO sorbents, enhances the risk of sulfidation and other forms of sulfur attack. Synergistic erosion/corrosion and deposition/corrosion interactions may favor the growth of erosion resistant oxides on blade surfaces, but brittle cracking of these oxides may be an important source of damage along heavy particle paths. In order to project turbine lifetime, it is essential that damage mechanisms be identified and localized with respect to position on the blade surface. For this reason, small-scale rotary tests which simulate the particle and gas flow dynamics

of larger turbines are useful intermediate tests between preliminary cascades and costly full scale operations in the assessment of turbine materials. This report summarizes the initial results of the NASA Lewis PFBC small-scale rotor program to date.

The NASA Lewis PFBC research program was initiated in 1976 to provide support for the Energy Research and Development Administration in the areas of coal combustion and turbine and materials technology. The facility was completed early in 1977, and the results of carrousel wedge tests performed in effluent directly from the bed with no gas cleanup were reported later that year. (3) Erosion was severe (2 to 60 cm/yr, .1 to 3 mil/hr) on the leading edge of the rotating wedge samples, but there is some indication that a protective oxide layer reduced erosion at low velocity on one alloy (IN 100). Conclusions reached in these earlier tests include: (1) there is little difference in the erosion behavior of nickel and cobalt based superalloys when eroded to bare metal; (2) at velocities from 150-270 m/s, erosion varied as $v^{2.5}$; and (3) sulfidation in PFB effluent was observed on all samples at temperatures of about 800 C (right and left faces), and on none of the samples at 720 C. The turbine tests were undertaken to explore erosion/corrosion interaction in PFB effluent at lower solids loadings and higher gas velocities in a simulated large-scale turbine environment.

## PFB TEST FACILITY

### Combustor

The research facility is shown in Figure 1. A conical bed (2.1 m x 0.4 m average dia) burns about 14 kg of coal per hour and about 1 kg of sorbent. Air flows at 300 kg/hr into the combustor. At these feed rates, the energy output is 120 kw (400,000 BTU/hr) and the top of bed temperature is about 1000 C. A small portion of the effluent from the top of the bed is continuously fed through steam jacketed lines to a gas analyzer in the control room. The hot gases flow upward through a single Aerodyne cyclone separator and into the turbine, which is located in a high bay area above the bed (Figure 2). Exhaust gases are cooled and pass through additional filters before exiting at a pressure valve on the roof. The bed pressure is maintained at about 5.5 atmospheres, and the pressure drop across the turbine is regulated by adjusting the exit valve. Solids are collected for analysis from a solids removal screw at the top of the bed, the cyclone separator, and a separator downstream from the turbine. All data acquisition and control systems are computerized.

### Turbine

The turbine is a modification of a single stage Chrysler automotive turbine. The integrally cast rotor is 14 cm in diameter and contains 53 blades. The automotive turbine was designed to operate at mass flows 10-15 times greater than that generated by the combustor. In order to accommodate the flow capacity of the rotor and to generate tip speeds comparable to utility turbine tip speeds ( 300 m/s), the turbine was

operated at 6% partial admission. Therefore, 2-3 blades are directly exposed to the high velocity effluent stream at a particular time. At a rotation speed of about 38,000 rpm, the turbine generates 5-8 hp with partial admission under the test conditions. The assembled turbine is shown in Figure 3.

The shaft of the rotor rests on air purged journal and thrust bearings (Figure 4). The relative position of the rotor disc and shaft in the automotive design is inverted from usual construction, so that the leading edge of the blades face the shaft. The stator opening is located in the housing near one of the bearings. In order to reach the stator inlet, the combustion gas line (5 cm dia) rising from the bed makes a 90 degree turn near the center of the shaft. A second turn of about 65 degrees in the stator and a reduction in flow area to about 1.3 $cm^2$ generates design velocities ($\simeq$ 500 m/s) at the stator exit. Assymetric erosion of the stator indicated that considerable heavy particle separation occurred at these turns.

A dual purpose air starter and brake operated with pressurized air regulates rotation speed. Maqnetic pickups produce the regulating speed signal, and two Bently proximity probes initiate shutdown if shaft alignment is disturbed. Oil and bearing temperatures are also incorporated in the automatic warning and shutdown system. Pressure taps are located near the knee of the gas inlet line, at the stator exit near the rotor tip, and in the rotor exit port. The turbine pressure ratio is automatically regulated from the stator inlet and rotor exit pressures (total-to-static). Snielded thermocouples are located at the stator inlet near the pipe wall.

## TEST CONDITIONS

### Gas and Turbine Parameters

The first two turbine runs R1 and R2, were terminated because of a leading edge rub on the housing (R1) and loss of a blade (R2). In the three tests included in this report, rotors were exposed to the effluent of three different coal/sorbent combinations - Pennsylvania coal No. 8 and limestone (Pa/lime), Ohio coal and dolomite (Ohio/dol), and Ohio coal and limestone (Ohio/lime). These combinations were chosen to test the sulfur removal effectiveness of the two sorbents and the feasibility of burning high sulfur Ohio coal in a PFBC.

Table 1 shows the gas composition and solids loading of the effluent prior to cleanup for R3 (Pa/lime), R4 (Ohio/dol) and R5 (Ohio/lime). Top of bed solids loading ranged from 1900 to 4100 ppm, and $SO_2$ content of the gas ranged from 110 to 670 ppm at steam temperature. The higher sulfur Ohio coal effluent contained both the greatest (with dolomite) and the least (with limestone) amount of $SO_2$, indicating that the action of the sorbent is important in determining gas composition. Both Ohio coal runs were made under nonadiabatic conditions. Water cooled rods in the bed simulated practical operating conditions in which both steam and effluent driven turbines would be linked to generators. With cooling rods

in the bed, solids carryover seemed to be considerably higher, and the quantity of material removed by the solids screw was small.

The rotors were cast with nickel based alloys in shell molds (Figure 5). Two of the three rotors were IN792+Hf (12% Cr, 6% Al, 4.5% Ti) and one was Alloy 713LC (12% Cr, 3% Al, 0.6% Ti). Both of these alloys form predominantly chromium and nickel oxides and spinels at test temperatures (690-780 C) in air. Gas flow conditions in the stator are shown in Table 2. The two high velocity (560 m/s), temperature (780 C), and loading (2700 ppm) tests were run with IN792+Hf rotors; the lower velocity (490 m/s), loading (600 ppm), and temperature (690 C) test was run with an Alloy 713LC rotor. Average cyclone efficiency ranged from 60 to 70% and was much higher at times during R3. Because of the difference in alloy composition, a direct comparison of high and low velocity erosion rates requires the assumption that the alloys behave similarly. This assumption, based on previous Lewis wedge test results, may be correct only if the erosion surfaces are similar or if a significant amount of loss is generated by the erosion of bare metal.

A turbine velocity diagram for R3 is shown in Figure 6. As potential energy which is stored in the pressure difference across the rotor is converted into kinetic energy and work, the velocity of the gas flow changes. The relative gas velocity at the stator exit (260 m/s at mean radius) accelerates to about 480 m/s at rotor exit. Because of drag forces, it is unlikely that heavier particles accelerate to velocities much greater than the leading edge velocity. The most erosive particles in these high solids loading tests are more likely to maintain forward momentum and gain additional momentum by impact from the rotor. Lighter particles, some of which are captured by and deposited on the blade, probably experience significant acceleration. Table 3 shows the relative gas inlet and exit velocities of the three rotors. Inlet relative velocities (260-330 m/s) were comparable to the velocity of the rotor at mean radius ($\simeq$275 m/s).

Particle Concentration and Size Distribution

Nonadiabatic burning of Ohio coal and dolomite generated the greatest amount of solids carryover from the bed. In addition, the particle size distribution appears to be significantly different from that of the other coal/sorbent combinations. Figure 7 shows the particle size distribution of samples taken at 3-8 hour intervals in the three tests. In comparison with Ohio coal and limestone solids at 2600 ppm, Ohio coal and dolomite solids contain more particles in the potentially erosive 20-40 u range. Within the range of measurement error, there appears to be little difference in particle size distribution between Ohio and Pennsylvania coal with limestone, despite the wide range of loadings. The number of particles with size greater than 30 u does appear to be enhanced at the highest loading. These size distributions are a function of both off-the-bed particulate size and cyclone separation characteristics. The Ohio/dolomite size distribution may reflect a lower cyclone efficiency in the 20-40 u range as a result of excessive carryover.

The solids chemical composition varied only slightly with coal and sorbent. Table 4 shows the chemical composition of solids which pass through the turbine in comparison with the composition of coal ash. The relative amounts of Si, Al, and Fe are similar to those found in coal ash. The larger quantity of lime in R5 (Ohio/Lime) probably reflects the larger total quantity of elutriated solids. Sulfur content in the solids reflects the $SO_2$ content of the gas and not the sulfur content of the coal. Sulfation of the particles may take place both in the bed and in the cooler downstream temperatures where alkali salts may condense on the particle surfaces.

Figure 8 shows solids particles adhering to chromium oxide scraped from the pressure side of an R4 blade. The oxide may be from the surface or may have been deposited, perhaps after erosive removal from another blade or surfaces upstream. The solids particles are generally fluffy with varying Al-Si, K, Ca, and Fe content. The presence of sulfur is often accompanied by K and Fe, suggesting the presence of alkali metal-iron trisulfates. The smooth, dark appearance of these regions may indicate previous melting. Large $CaSO_4$ crystals imbedded on the oxide are representitive of highly erosive species.

## RESULTS AND DISCUSSION

### General

Erosion, corrosion, and deposition varied with position on the exposed blades. The absolute loss in blade thickness was measured at various positions on the blade surface. Erosion to bare metal occurred at heavy particle impact sites on the leading edge, pressure side and trailing edge tip, and deposits formed primarily at lighter particle impact sites on the suction side and behind the leading edge. Deposition was minimal on the most highly eroded blades ($<$1u). Evidence of accelerated oxide growth (10 to 100 X air) and atypical oxides (sulfur-rich, subsurface, chromium depleted) were present on even the most severely eroded blades.

Table 5 summarizes the erosion rates and typical oxide morphologies for the three turbine tests. The presence of enhanced oxidation on severely eroded samples supports the theory that erosion/corrosion interactions may favor the growth of hard oxides. Since both deposition and oxide growth occurred primarily on the suction side of R3 blades, a deposition/corrosion synergism may exist as well.(4) The erosion surfaces of R3 and R5 blades were similar (40-50% bare metal), despite a large difference in erosion rate; the surfaces of R4 blades were almost completely eroded to base alloy or exposed depletion zones (90% bare metal) at an erosion rate only twice as great as the R5 rate. The evolution of the erosion surface appears to be a complex function of material, time, temperature, local erosion rate, and the composition and coherence of deposits.

## Erosion

Severe erosion sites along heavy particle paths were highly visible and reflect centrifuging of particles after impact at the leading edge. Particle separation generated at large-angle turns in the gas flow direction immediately before and in the stator focused a stream of heavy particles on the rotor near the hub. A notch in the stator carved by the heavy particle stream corresponded, in each test, to a notch in the blade leading edges. Further centrifugal separation after impact with the rotor produced clearly distinguishable areas of light and heavy particle damage on the blade surface.

Average surface materials loss on the Alloy 713 LC rotor (R3) was 0.1 mm (4 mils) and the loss rate was about 0.6 u/hr (0.024 mil/hr). Leading edge to trailing edge losses were comparable. Figure 9 shows the erosion and deposition pattern on an R3 blade. After rebounding from the leading edge, some heavy particles appear to impact on the pressure side of the blade above as they are thrown radially outward, finally impacting a third time on the trailing edge tip. The rippled appearance of erosion on the pressure side (Figure 10) is evidence of impact at the maximum erosion angle ($\simeq$ 30 degrees) (5). Average erosion loss rates projected from small-scale turbine tests are likely to be conservative because of the higher probability of multiple impact with smaller blade separations. A larger centrifugal force in small radius rotors also enhances erosion near the tip. Deposition occurred on areas surrounding the heavy particle path primarily on the suction side.

R4 was terminated by complete loss of the blades after 13 hours. Erosion damage had severely weakened the structure of the blades, and examination of the blade fragments revealed that many were joined to the root at a single point near the leading edge (Figure 11) prior to failure. Average surface loss, estimated from blade fragments, was 0.25 mm (10 mils) and the loss rate was 18 u/hr (0.7 mil/hr). The location of sites of heavy metal loss is consistent with the leading edge notch and teardrop shaped pressure side erosion observed on R3 blades. After 12 hours at nearly the same high solids loading, R5 blades had lost only the trailing edge tip section. Average surface loss (0.1 u, 4 mils) and erosion rates (8.5 u/hr, 0.3 mil/hr) were less than half as great as R4 losses.

A comparison of surface loss rates projected for full admission is shown in Figure 12. At 6% partial admission, the exposure times are equivalent to 10 hours for R3 and about 0.75 hours for R4 and R5. In these times, the average loss rate ranged from 10 to 300 u/hr (0.4 to 12 mil/hr). Both R3 and R5 rotors were exposed to limestone sorbent effluent. The normalized erosion rate of R5 (45 cm/yr/1000 ppm, 3.8 (mils/hr)/(gr/SCF)) is three times greater than that of R3 (15 cm/yr/1000 ppm, 1.3 (mils/hr)/(gr/SCF)). If erosion varies as the cube of velocity, the erosion rate should be only twice as great at the higher velocity. The additional factor may reflect a larger proportion of heavy particles at higher solids loading, a slight difference in particle composition, or a difference in the erosion resistance of the oxide or metallic surfaces.

Nonlinearity with loading may be expected if erosion varies as particle size (6), since a larger proportion of heavy particles impacted R5 blades. The morphology of the oxide surface is also different, as may be seen from microscopic examination.

The difference in R4 and R5 erosion rates, both Ohio coal runs, reflects only the change of sorbent from dolomite to limestone. Since the solids chemical composition is not significantly different, a larger average particle size may be responsible for the catastrophically greater erosion damage with dolomite. On the basis of these tests, average surface loss rates with Pennsylvania coal and limestone at a solids loading of 20 ppm (0.01 gr/SCF) would be about 3 mm/yr (13 mil/1000 hrs) if particles impact at 260 m/s. Maximum damage sites on the blade will be determined by the blade shape and particle dynamics. This estimate could be several orders of magnitude high if a more erosion resistant oxide surface is generated at lower loadings and if the particle size distribution changes significantly.

Corrosion

The suction side was the primary site of coherent oxide formation on R3 and R5 blades, and exposed depletion zones were present on all but the most highly eroded surfaces on R4 blades. Figure 13 shows the suction side surfaces of test rotor blades in comparison with the surfaces of oxidation coupons exposed to air in a furnace test for similar times at temperature. The depth of oxide affected layers on the turbine blades (5-10 u) is significantly greater. In addition, X-ray analysis indicates that IN792+Hf blade oxides contained a larger proportion of aluminum than the air-oxidized sample oxides, which also contained relatively large quantities of chromium and nickel. The delicate balance between alloy composition, gas composition and temperature which favors the growth of thin, protective oxide layers appears to have been disrupted in the aggressive PFB effluent environment.

The oxidation pattern of an Alloy 713 LC blade, exposed for 164 hours at 690 C, is shown in Figure 14. Oxide affected layers of about 10 u are seen on most of the suction side beneath 1-2 u deposition layers. The average erosion depth is an order of magnitude greater than the average oxidation affected depth. Oxides on the suction side are typically rich in chromium (Figure 15) and may be protective unless erosively damaged by brittle cracking (Figure 16).

Toward the trailing edge, the oxides change in appearance and composition. The metal matrix is retained, there is no visible depletion zone, and X-ray analysis indicates that the oxide is rich in both chromium and sulfur (Figure 17). No other deposition solids (e.g. Ca,K) are present beneath the surface. Oxides formed in $SO_2/O_2$ atmospheres have previously been described in which particles of chromium depleted metal are imbedded in a chromium oxide matrix (7), and oxides and sulfides can be highly intermixed if formed at the scale/gas phase boundary (8). However, the partial pressure of $SO_x$ in PFBC effluent is typically too low to support these mechanisms; and the reason for reaction rate

limitation at the scale/gas interface, if such is the case, is uncertain. Deposition materials containing potassium iron trisulfate ($K_3Fe(SO_4)_3$) or other sulfates are a possible source of sulfur (9). $SO_2$ pressures beneath coherent deposit layers may be sufficiently high to permit some form of sulfur penetration. Microprobe analysis reveals a coherent iron bearing deposition layer on the surface above the sulfur-rich Cr oxide, and visible deposition near the trailing edge has the dark, glassy appearance of fused trisulfates.

On the pressure side, oxide growth is irregular and deposition is heavy ($\simeq$10u). In some areas, Cr oxides are mixed with deposition materials in the absence of visible depletion zones (Figure 18). This buildup may be primarly composed of rebound particles from the leading edge of another blade. The formation of heavy deposits may also be protective against erosion, but heavy deposits do not necessarily enhance oxide or sulfide growth.

Oxides on heavily eroded R4 (IN792+Hf) blades, exposed for 13 hours at 780 C, were limited to projecting aluminum and titanium oxide nuclei with substrate oxide streamers in broad ($\simeq$ 10u) depletion zones (Figure 19). Remnants of Cr and Ni rich oxides surrounding the nuclei or knobs suggest an oxide evolution picture in which harder subsurface aluminum oxide deposits either remain after surface oxides are eroded away or form in exposed depletion zones. Aluminum rich knobs seen on the pressure side of an R4 blade (Figure 20) may correspond to similar knobs observed on previous Lewis wedge bar tests with IN792. Deposition materials form a wake behind the knobs. Since the erosion rate of these blades was extremely high, the presence of highly localized aluminum oxide deposits does not appear to diminish the erosion rate. The relatively rapid formation of subsurface oxides after erosive removal of protective oxide elements may, in itself, be a materials problem at lower loadings.

R5 blades (IN792+Hf), also exposed at 780 C for 12 hours, contained a somewhat more protective oxide layer on the suction side. Aluminum rich deposits formed beneath chrome and titanium rich overlayers (Figure 21). The apparent presence of Hf and Ti carbides imbedded in mixed oxides on both R4 (Figure 22) and R5 blades suggest that carburization may also occur in the primarily oxidizing PFB effluent under deposition layers (10). The carbides are often seen rimming an oxide region.

## CONCLUDING REMARKS

Small-scale rotary turbine tests operated at partial admission provide materials information complementary to that derived from static tests, including:

1. the location of potentially heavy erosion sites consistent with heavy particle separation;

2. a conservative projection of full size turbine erosion damage on pressure and suction side surfaces;

3. the delineation of deposition sites consistent with turbine gas flow dynamics;

4. a spectrum of deposition/erosion/corrosion interaction pictures for each material which identifies potentially destructive and protective interactions.

Reliable scaling requires attention to blade spacing, blade length, and rotation speed relative to the average particle speed.

The separation of light and heavy particle damage paths by centrifuging in these tests permits an extrapolation of erosion/corrosion results to lower particulate loadings. At lower loadings (< 200 ppm, 0.1 gr/SCF), a large percentage of the blade surface may be covered with oxides similar to those seen on the suction side of blades in these turbine tests. Centrifugal separation and direct heavy particle impact will be reduced if the average particle size is smaller, and damage along heavy particle paths will likely be the result of brittle cracking or atypical oxide formation rather than erosion to bare metal. Sites of enhanced oxide formation may be protective against further erosion or they may be primary sites of damage from sulfur penetration or subsurface oxide formation. At even lower targeted solids loadings (< 20 ppm, 0.01 gr/SCF) the location and morphology of atypical oxides and sulfides may be important parameters in the selection of turbine materials and blade design.

The spectrum of oxidation schemes observed in these tests as a function of alloy, erosion rate, and blade position emphasizes the importance of understanding the dynamics of erosion/corrosion interaction in a rotating turbine environment for adequate materials damage and lifetime projections.

SUMMARY OF RESULTS

1. Small scale turbine tests provide realistic information about the location of oxidation, deposition and heavy erosion sites on the blade surface, as well as a conservative projection of large scale turbine erosion damage.

2. Heavy erosion (5 to 500 cm/yr, 0.2 to 20 mil/hr) occurred on blade surfaces at moderate to high solids loadings (600 to 2800 ppm, 0.3 to 1.5 gr/SCF) and typical utility turbine inlet velocities (260 to 330 m/s, 800 to 1000 ft/s). Dolomite sorbent and Ohio coal flyash may be more erosive than limestone sorbent and Pennsylvania coal ash.

3. Centrifugal particle separation resulted in enhanced erosion at a leading edge notch, on most of the pressure side, and on the suction side trailing edge near the tip. Deposition of lighter particles occurred primarily on the suction side and near the leading edge on the pressure side.

4. The formation of erosion resistant and nonresistant oxides on eroded

blade surfaces may be an important factor in determining ultimate turbine lifetime. The location and morphology of oxides appears to be a function of:

a. Local erosion rate

b. Composition and coherence of deposits

in addition to time, temperature, and alloy material.

5. Accelerated growth of protective surface oxides may prolong turbine life at low erosion rates. Coherent oxides (5-10u) were seen primarily on the suction side of Alloy 713LC (Cr and Ni) and IN792+Hf (Al and Ti) blades.

6. Oxides which form beneath coherent deposits (sulfur-rich oxides on Alloy 713LC) or near regions of heavy erosion (subsurface, localized, and cracked oxides on IN792+Hf) may be nonprotective and reduce turbine lifetime. Heavy particle paths may, therefore, be primary degradation sites even at lower loadings where erosion to bare metal is minimal.

REFERENCES


1. A. P. Fraas, "Survey of Turbine Bucket Erosion, Deposits, and Corrosion", ASME Paper No. 76-GT-123 (March 1975).

2. W. Tabakoff, "Erosion Study on Turbomachinery Affected by Coal and Ash Particles, Phase I Annual Report, DOE Contract EX-76-C-01-2465, (January 1978).

3. G. R. Zellars, A. P. Rowe, and C. E. Lowell, "Erosion/Corrosion of Turbine Airfoil Materials in the High-Velocity Fffluent of a Pressurized Fluidized Coal Combustor", NASA TP 1274 (July 1978).

4. D. E. Rosner, K. Seshadri, J. Fernandez, De La Mora, G. C. Fryburg, F. J. Kohl, C. A. Stearns, and G. J. Santoro,"Transport,Thermodynamics, and Kinetic Aspects of Salt/Ash Deposition Rates from Combustion Gases", 10th Materials Research Symposium", Characterization of High Temperature Vapors and Gases, NBS, Gaithersburg, Md (September, 1978).

5. I. Finnie and Y. H. Kabil, Wear, 8, 60 (1965).

6. W. F. Adler, "Preliminary Survey of the Literature on Solid Particle Erosion", to be published.

7. J. Stringer, "High Temperature Corrosion in Fluidized Bed Combustion", in Ash Deposits and Corrosion Due to Impurities in Combustion Gases (R. Byers, ed.), McGraw-Hill, NY (1978).

8. A Rahmel, "Kinetic Conditions for the Simultaneous Formation of Oxide and Sulfide in Reactions of Iron with Gases Containing Sulfur and Oxygen or Their Compounds", Corr. Sci., 13, (1973).

9. D. L. Douglass, and V. J. Bhide, "Mechanisms of Corrosion of Structural Materials in Contact with Coal Chars in Coal Gasifier Atmospheres", Semi-Annual Progress Report, DOE Contract EY-76-S-03-0034 (February 1978).

10. J. Perkins and A. Goldberg, "Behavior of Oxide Films on High-Temperature Alloys in Carbonaceous Gas Atmospheres", Oxid. of Metals, 11, 1 (1977).

TABLE 1. - ANALYSES OF COMBUSTOR EFFLUENT

| Run | Coal | Sorbent | Average effluent gas temperature | | Average solids loading | | Average gas composition[a] | | | | | |
|---|---|---|---|---|---|---|---|---|---|---|---|---|
| | | | C | F | ppm | gr/SCF | $O_2$ (percent) | $CO_2$ (percent) | CO (ppm) | $NO_x$ (ppm) | $SO_2$ (ppm) | THC (ppm) |
| R3 | Pa | Limestone | 860 | 1580 | 1900 | 1.0 | 11.4 | 8.3 | 11 | 244 | 218 | 1 |
| R4 | Ohio | Dolomite | 904 | 1660 | 7300 | 3.9 | 6.0 | 13.0 | 26 | 165 | 669 | - |
| R5 | Pa | Limestone | 880 | 1616 | 4100 | 2.2 | 6.8 | 12.9 | 28 | 133 | 112 | 1 |

[a]Analyses determined at steam temperature.



TABLE 2. - AVERAGE GAS FLOW CONDITIONS ON THE STATOR

| Turbine run | Inlet pressure[a] (atm) | Inlet temperature C | Exit velocity (m/s) | Solids Loadings | | Mass flow Kg/hr |
|---|---|---|---|---|---|---|
| | | | | (ppm) | (gr/SCF) | |
| R3 | 5.4 | 690 | 490 | 600[b] | 0.3 | 285 |
| R4 | 5.4 | 780 | 560 | 2800 | 1.5 | 290 |
| R5 | 5.6 | 780 | 560 | 2600 | 1.4 | 290 |

[a]Approximate total pressure.

[b]Daily solids loadings ranged from 20 ppm to 2500 ppm in the 164 hour test.

TABLE 3. - AVERAGE TURBINE TEST CONDITIONS

| Turbine run | Rotor material | Exit pressure (atm) | Pressure[a] ratio | Relative gas velocity | | Rotor speed | | Run time (hrs) |
|---|---|---|---|---|---|---|---|---|
| | | | | Rotor Inlet (m/s) | Rotor Exit (m/s) | 1000 rpm | m/s | |
| R3 | Alloy 713 LC | 2.8 | 1.95 | 260 | 480 | 40 | 280 | 164 |
| R4 | IN 792 + Hf | 2.8 | 1.95 | 330 | 480 | 38 | 265 | 13 |
| R5 | IN 792 + Hf | 2.9 | 1.95 | 330 | 480 | 39 | 270 | 12 |

[a]Stator-inlet total pressure to rotor-exit static pressure.

TABLE 4. - COMPARISON OF COMPOSITION OF SOLIDS THROUGH THE TURBINE WITH COAL ASH COMPOSITION

| Constituent | PFE Solids | | | Coal Ash | |
|---|---|---|---|---|---|
| | R3 [illegible]/Limestone | R4 Ohio/Dolomite | R5 Ohio/Limestone | PA (Total = 7.94%) | Ohio (Total = 9.95%) |
| | Wt % | | | Wt % of ash | |
| Silica | 33 | 37 | 38 | 47 | 47 |
| Alumina | 19 | 19 | 19 | 25 | 25 |
| Ferric Oxide | 18 | 12 | 11 | 17 | 22 |
| Lime | 7 | 10 | 22 | 4 | 1 |
| Magnesia | 1 | 5 | 2 | 1 | 1 |
| | Wt % | | | Wt % of coal | |
| Sulfur | 2.69 | 4.00 | 2.00 | 1.9 | 2.4 |

TABLE 5. - SUMMARY OF EROSION/CORROSION RESULTS

| Test | Material | Test time (hrs) | Inlet gas temperature (C) | Relative[a] gas velocity (m/s) | Coal | Sorbent | Average solid loading (ppm) | Average erosion rate (μ/hr) | Erosion to bare metal (% of surface area) | Suction side oxidation depth (μ) | Oxide morphology |
|---|---|---|---|---|---|---|---|---|---|---|---|
| R3 | Alloy 713 LC | 164 | 690 | 260 | PA | Limestone | 600 | 0.6 | 40 | 5-10 | Primarily Cr-Ni rich oxides<br>Sulfur-rich Cr oxides |
| R4 | IN 792 + Hf | 13 | 780 | 330 | Ohio | Dolomite | 600 | 18 | 90 | 5-10 | Al-Ti oxide nucleii and sub-surface streamers in depletion zones. |
| R5 | IN 792 + Hf | 12 | 780 | 330 | Ohio | Limestone | 800 | 8.5 | 50 | 5-10 | Cr-Ti rich surface layers<br>Al-rich subsurface oxides |

[a]At rotor inlet.

[b]Includes thin (<1μ) oxides; estimated from 750 x cross-section photographs and visual examination.



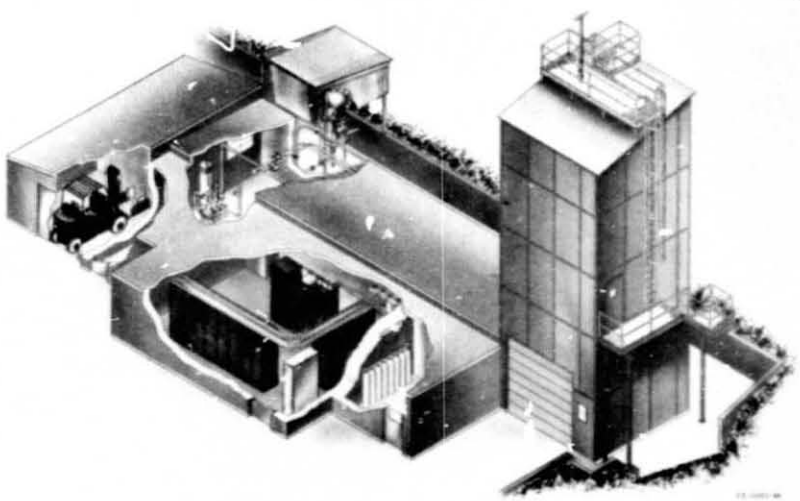

Figure 1. - Lewis pressurized fluidized bed test facility.

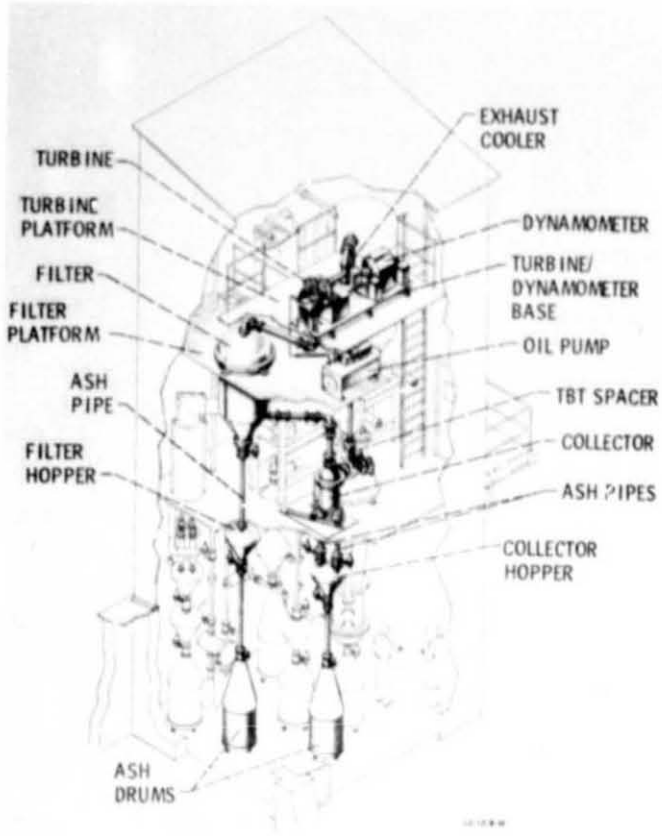


Figure 2. - High bay test area.

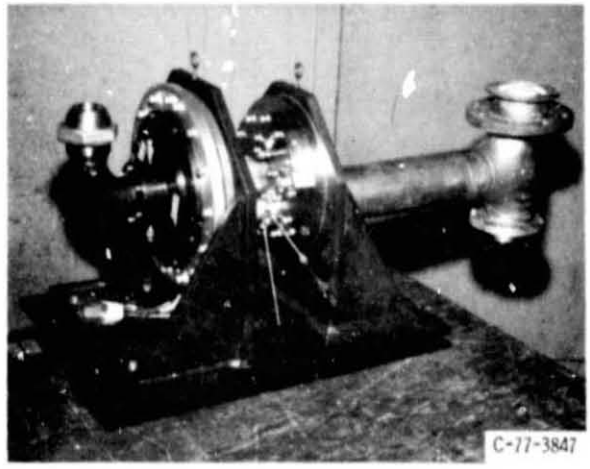


Figure 3. - Assembled turbine.

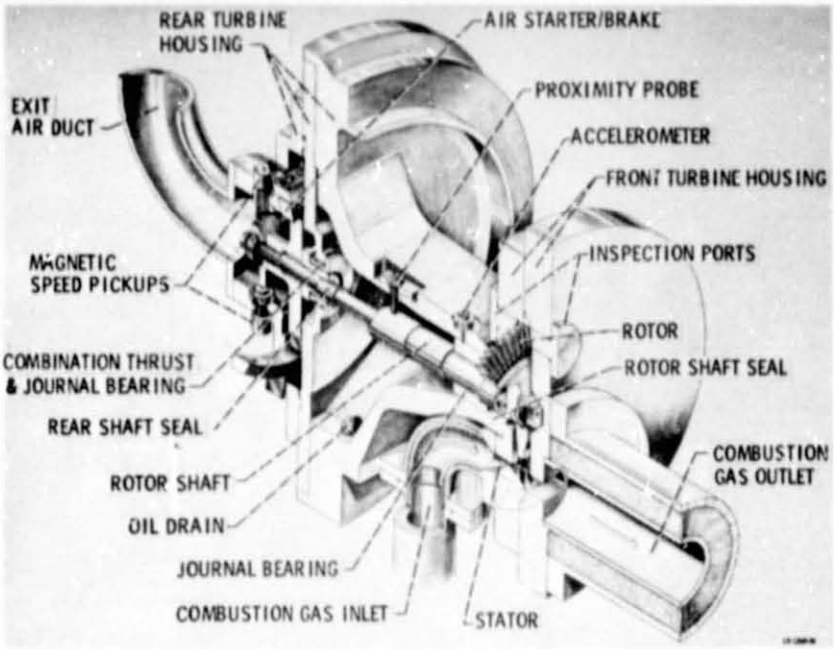


Figure 4. - Isometric sectional drawing of turbine.



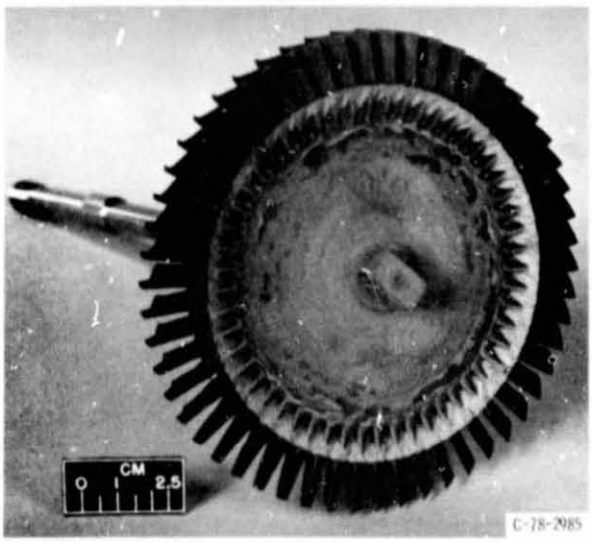


Figure 5. - Cast rotor with shaft.

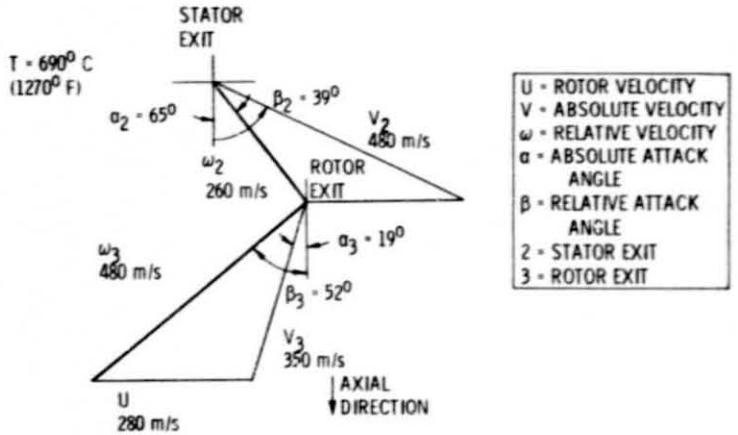


Figure 6. - Typical turbine gas velocity diagram for R3 at mean radius.

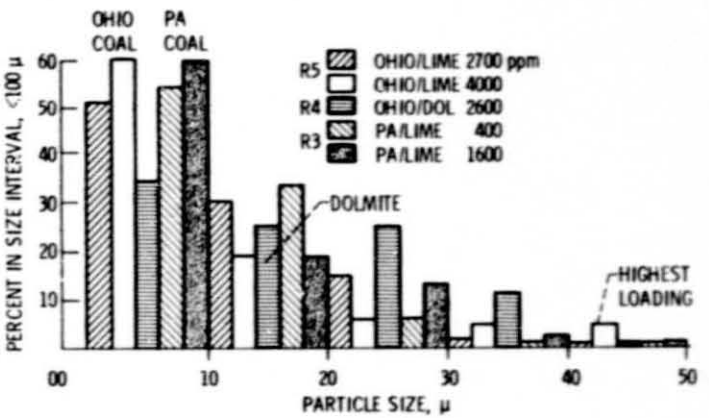


Figure 7. - Typical size analysis of solids loading into the turbine during 3 to 8 hour collection times.



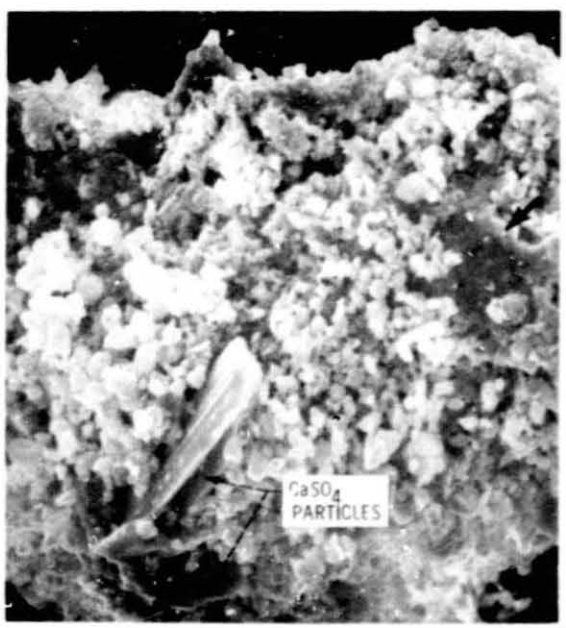


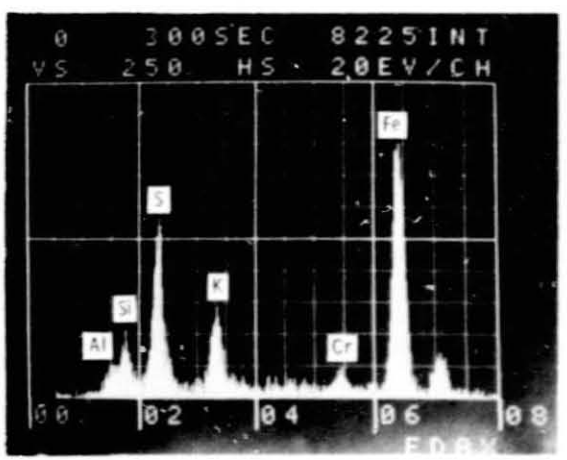


Figure 8. - Solids particles adhering to chromium oxide.

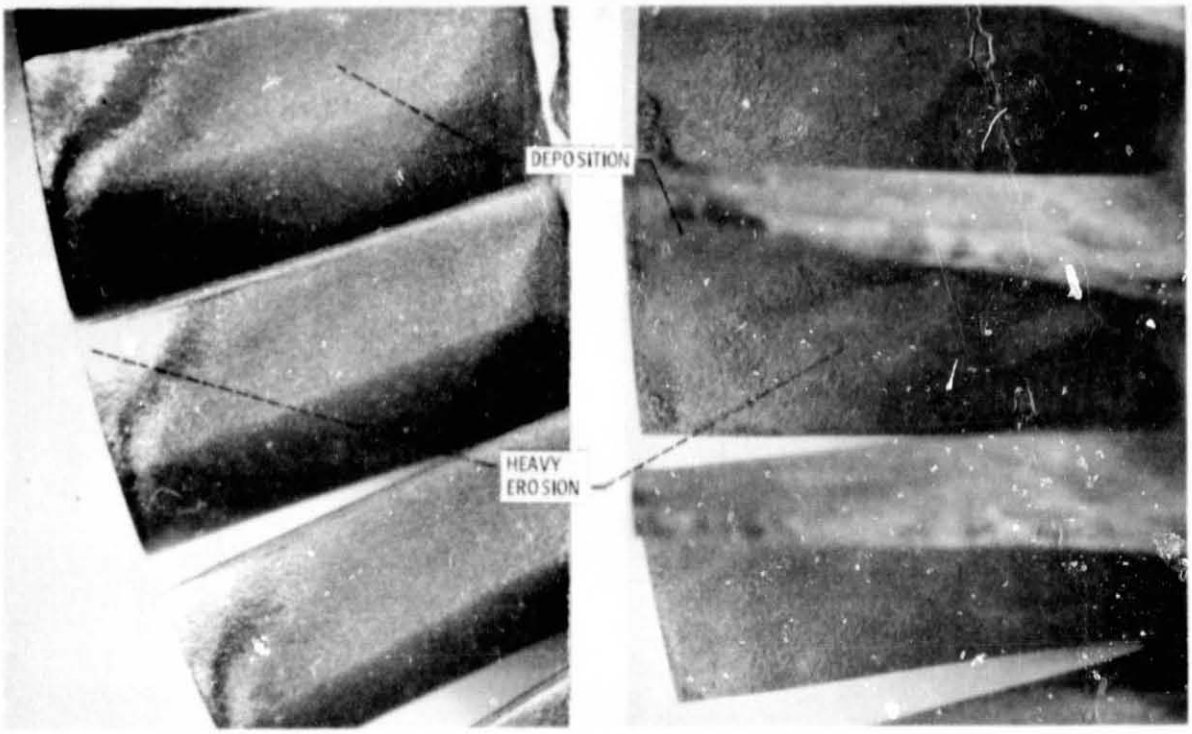


ROTOR 3, Pa COAL/LIMESTONE

Figure 9. - Erosion of alloy 713 LC exposed at 260 m/sec, 690° C, 164 hours. Solids loading = 600 ppm (0.3 gr/SCF).

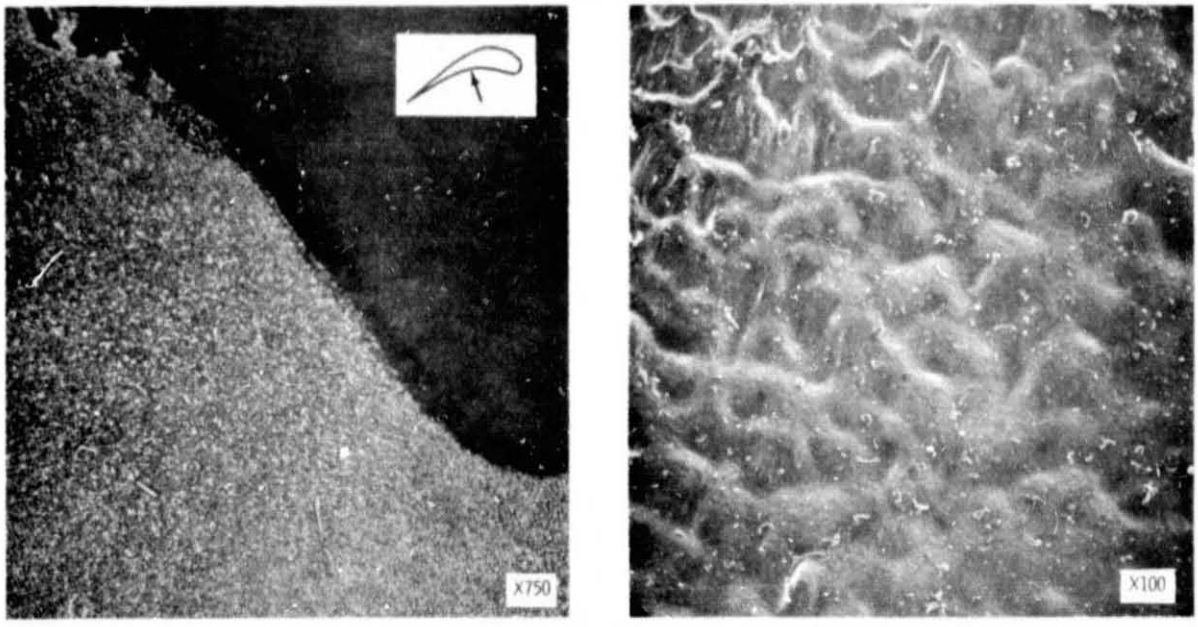


Figure 10. - Rippled appearance of pressure side erosion on alloy 713 LC (R3).

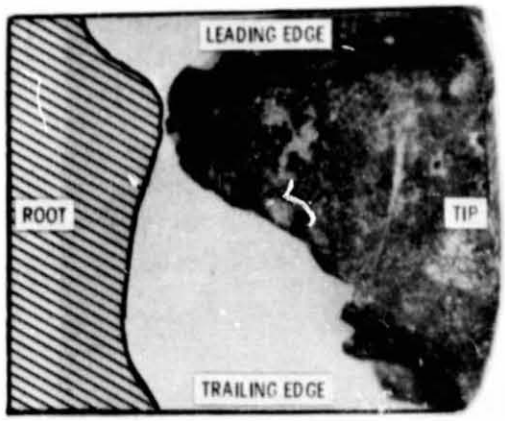


ROTOR 4, OHIO COAL/DOLOMITE

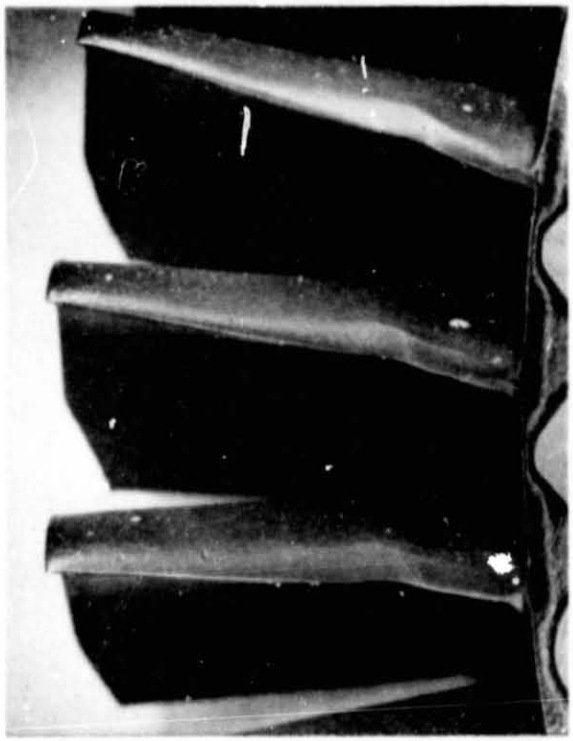

ROTOR 5, OHIO COAL/LIMESTONE

Figure 11. - Erosion of IN 792 + Hf blades at 330 m/sec, 780° C, 12-13 hours. Solids loading, ≈ 2700 ppm (1.5 gr/SCF).

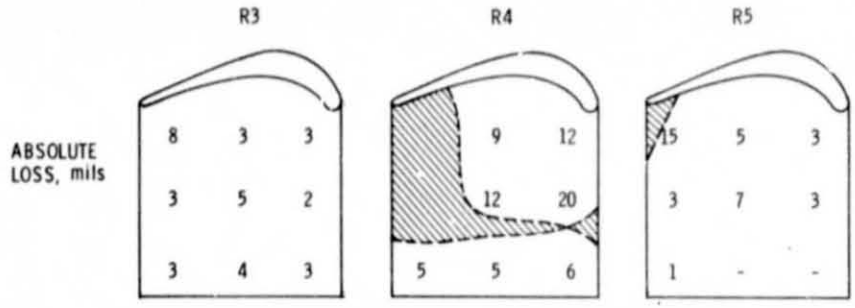


| | R3 | R4 | R5 |
|---|---|---|---|
| RELATIVE VELOCITY, m/s | 260 | 330 | 330 |
| EQUIVALENT TIME, hr | 10 | 0.78 | 0.72 |
| SOLIDS LOADING, gr/SCF | 0.3 | 1.4 | 1.5 |
| PROJECTED NORMALIZED LOSS RATE, (mils/hr)/(gr/SCF) | 1.3 | 8.9 | 3.8 |
| AVERAGE LOSS RATE, (mil/hr) | 0.4 | 13 | 5.7 |

1 mil = 25.4 μ; 1 mil/hr = 22 cm/yr
1 (mil/hr)/(g/SCF) = 12 (cm/yr)/1000 ppm

Figure 12. - Projected surface erosion loss rate at full admission.

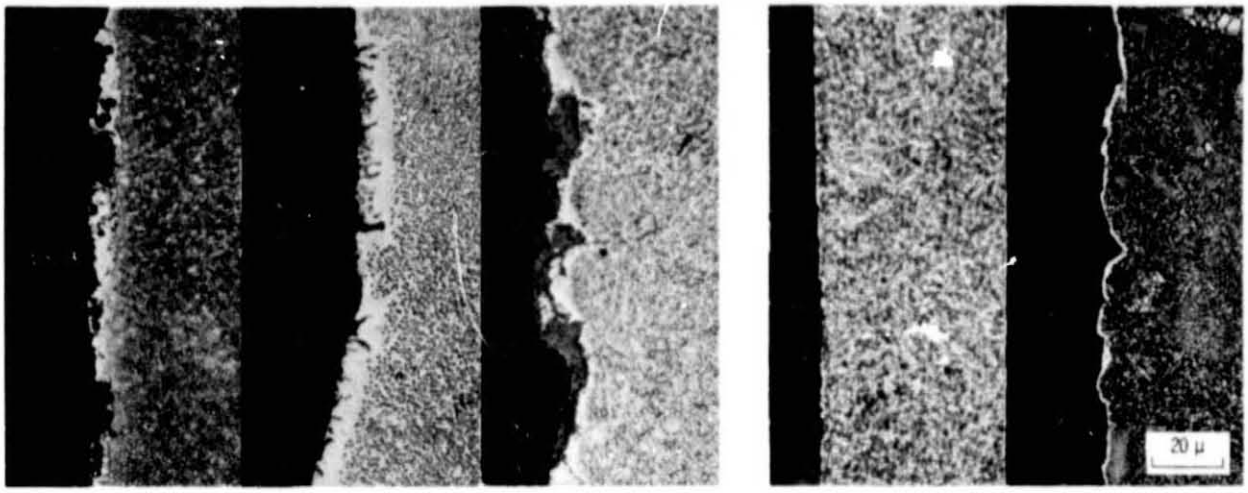


ALLOY 713 LC, R3, 690° C, 164 HOURS

IN 792 + Hf, R4, 780° C, 13 HOURS

IN 792 + Hf, R5, 780° C, 12 HOURS

EXPOSED TO PFB EFFLUENT

ALLOY 713 LC, COUPON, 704° C, 164 HOURS

IN 792 + Hf, COUPON, 816° C, 12 HOURS

AIR OXIDIZED

Figure 13. - Suction side oxidation compared with furnace oxidized coupons.

E-125

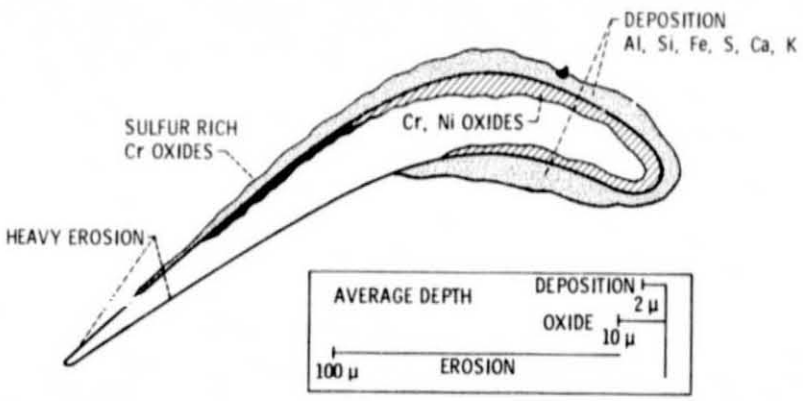


Figure 14. - Erosion/corrosion schematic of an alloy 713 LC blade; tip section (R3).

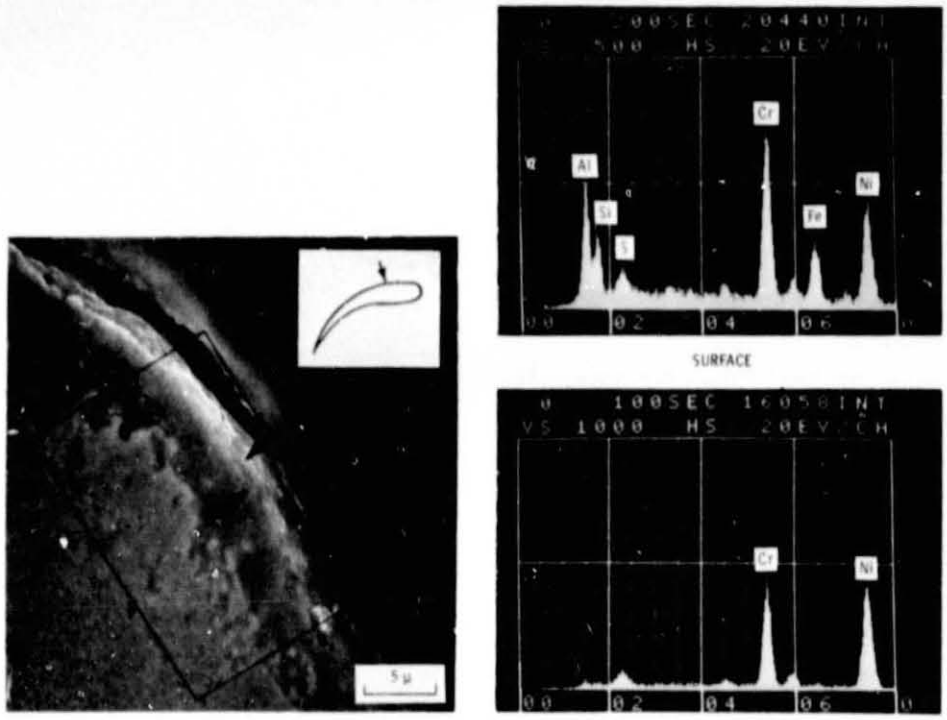


Figure 15. - Chromium-rich oxide on alloy 713 LC blade, exposed at 690° C for 164 hours (R3). Erosion rate, 0.6 μ/hr (0.024 mil/hr).

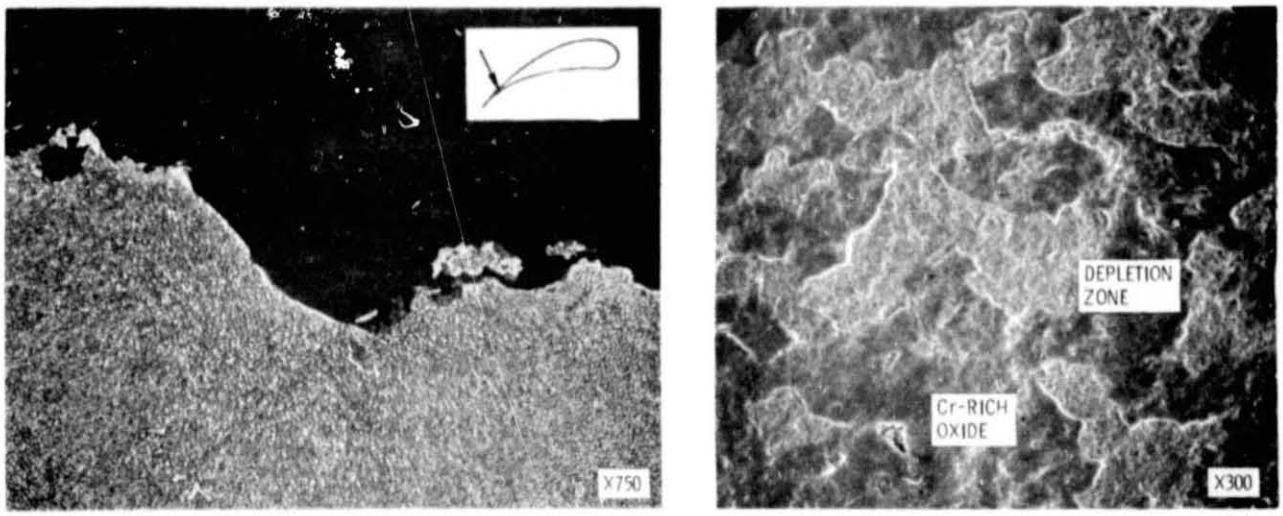


Figure 16. - Erosion of protective oxide layers in transition zones on alloy 713 LC (R3).

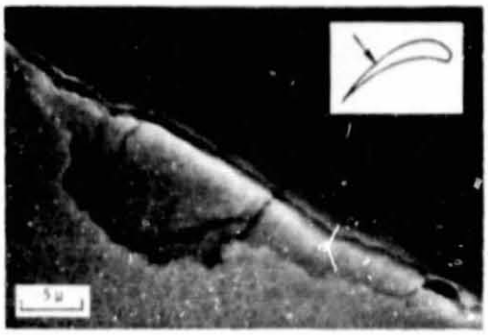


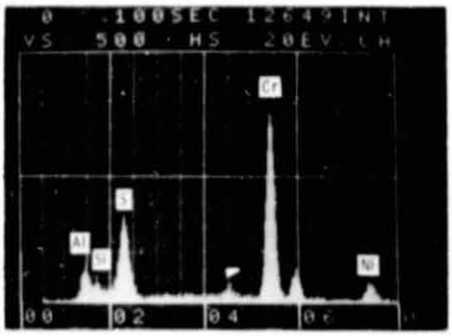


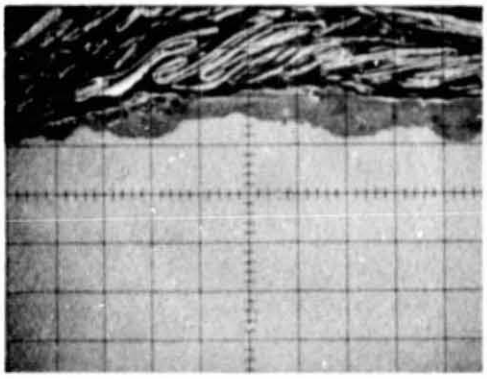

SECONDARY ELECTRON IMAGE

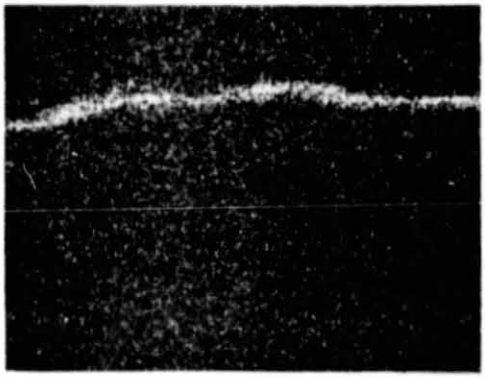

IRON

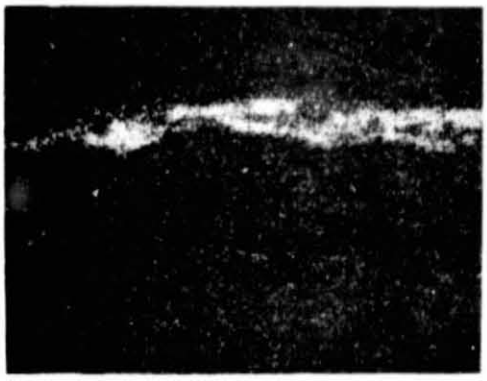

SULFUR

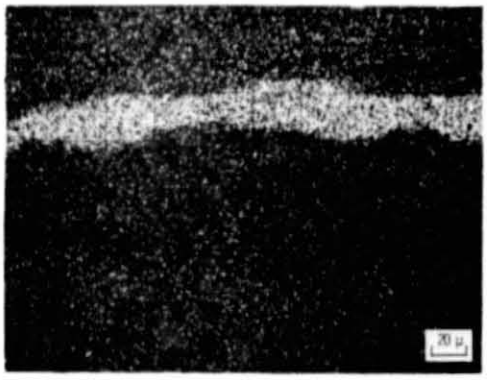


OXYGEN

MICROPROBE X-RAY ANALYSIS

Figure 17. - Sulfur-rich chrome oxide on suction side of an alloy 713 LC blade, exposed at 690° C for 164 hours (R3).

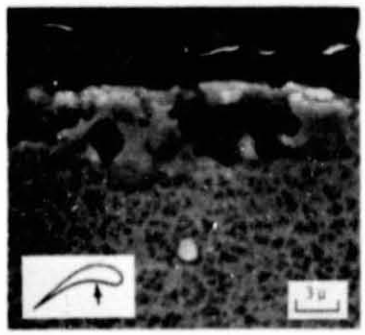


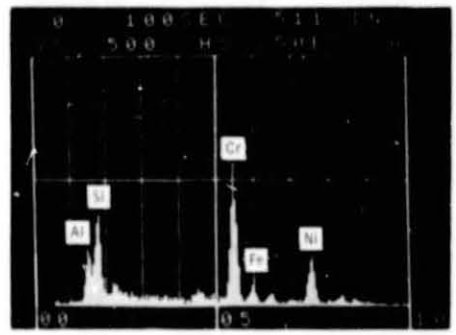


DARK AREA

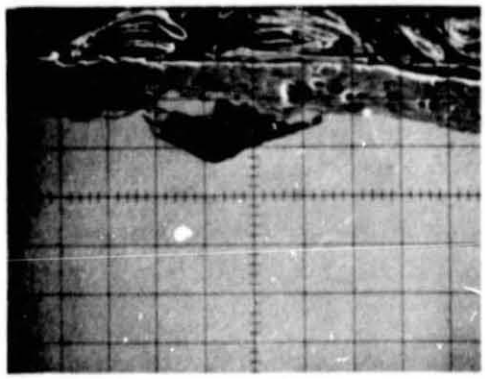

SECONDARY ELECTRON IMAGE

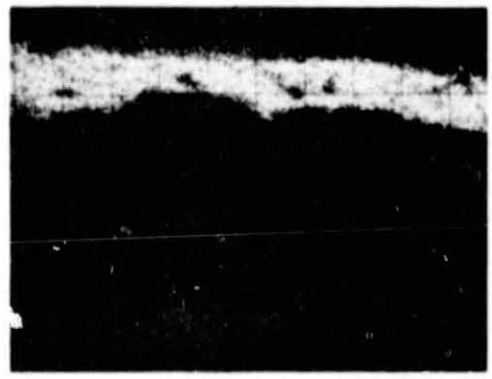

IRON

ALUMINUM

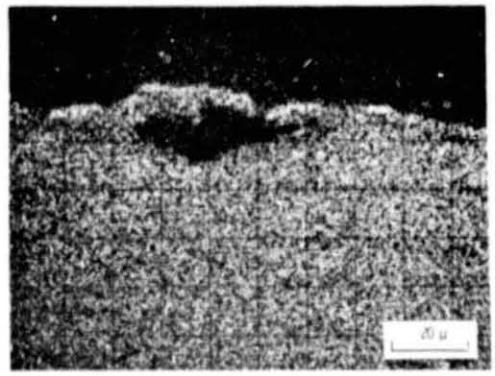


CHROMIUM

MICROPROBE X-RAY ANALYSIS

Figure 18. - Heavy pressure side deposition on alloy 713 LC blade (R3).

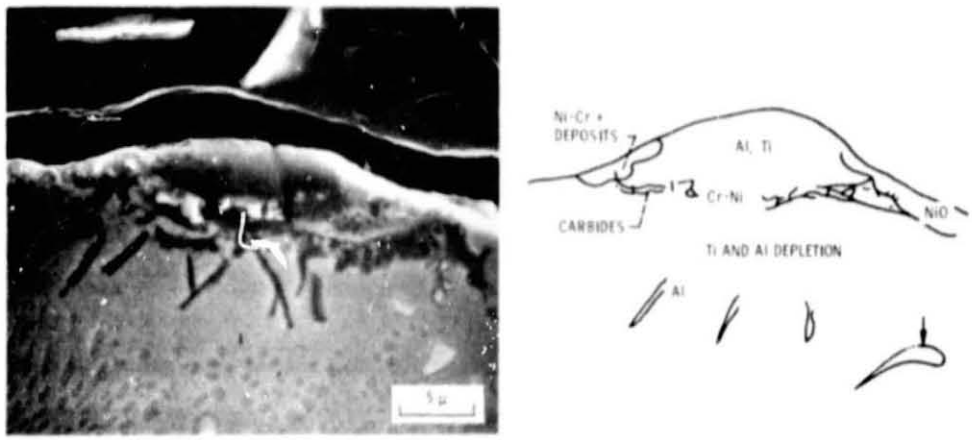


Figure 19. - Aluminum and titanium rich oxide on IN 792 + Hf blade, exposed at 780° C for 13 hours (R4). Erosion rate, 18 μ/hr (0.7 mil/hr).



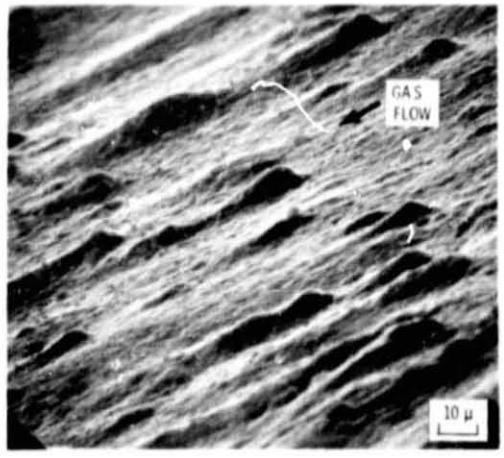


Figure 20. - Aluminum-rich knobs on pressure side of an IN 792 + Hf blade (R4).

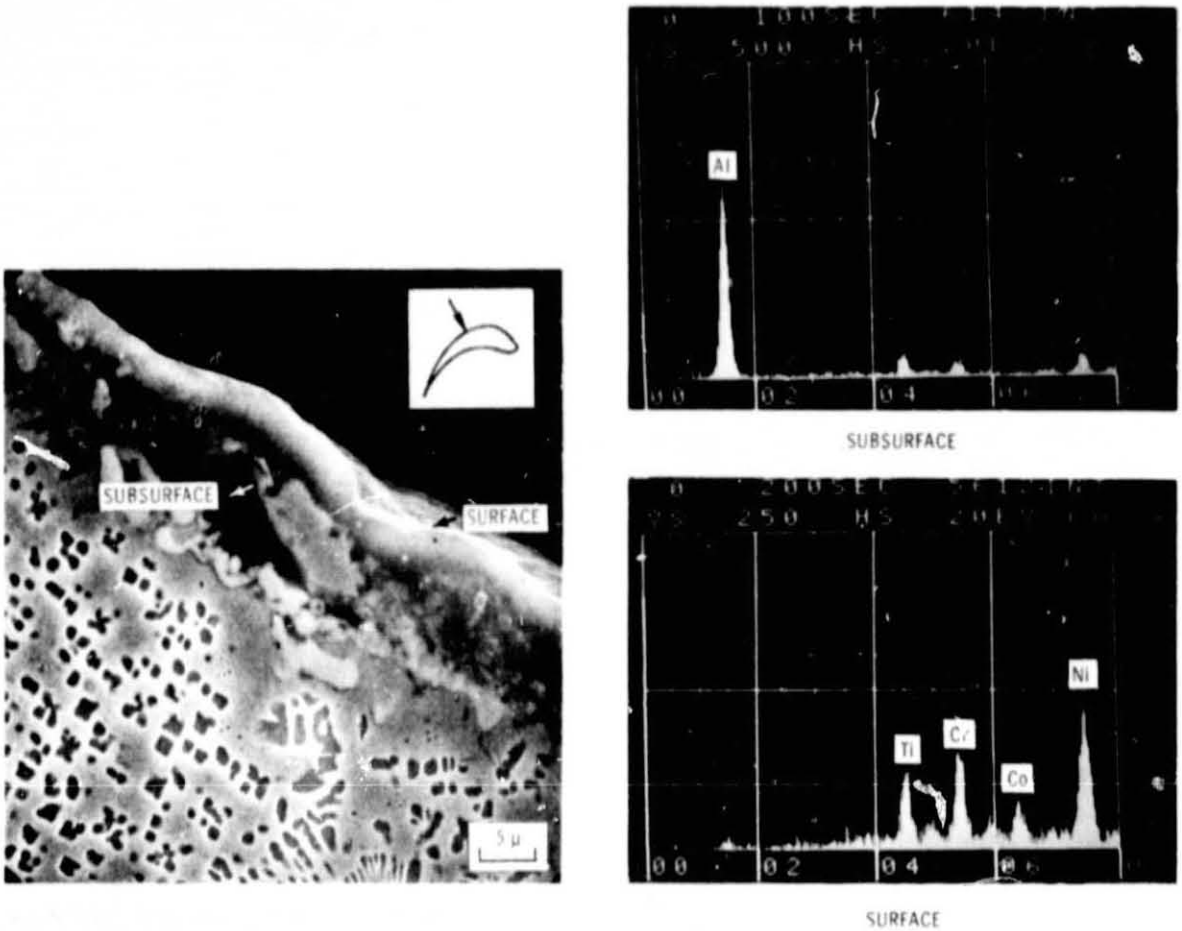


Figure 21. - Aluminum, chromium, and titanium rich oxides on IN 792 + Hf blade, exposed at 780° C for 12 hours (R5). Erosion rate, 8.5 μ/hr (0.32 mil/hr).



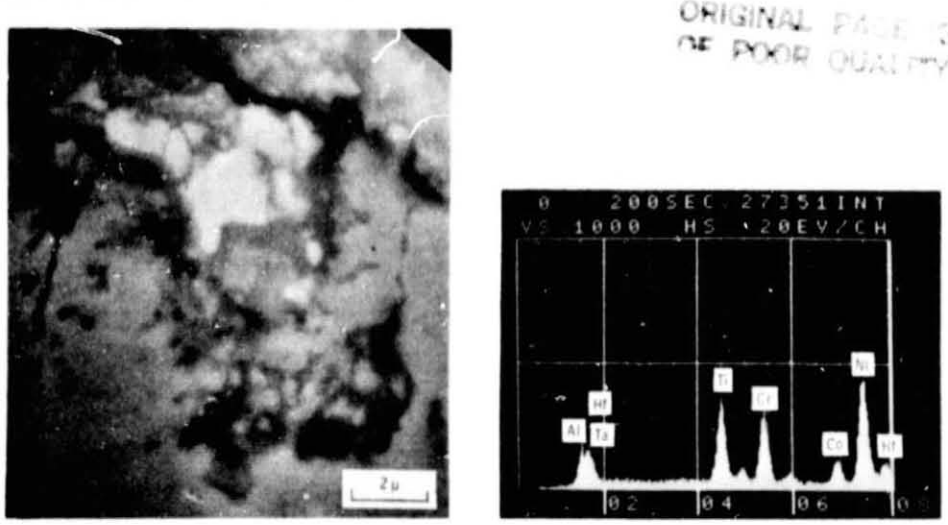


Figure 22. - Carbides imbedded in mixed oxides on IN-792 + Hf blade (R4).